NANO LETTERS

pubs.acs.org/NanoLett
Letter

Plasmonic Hinge Modes in Metal-Coated Nanolasers

Sangyeon Cho, Yi Yang, Marin Soljačić, and Seok Hyun Yun*

Cite This: *Nano Lett.* 2024, 24, 13647−13652
Read Online

ABSTRACT: Plasmonic lasers have traditionally been built on flat metal substrates. Here, we introduce substrate-free plasmonic lasers created by coating semiconductor particles with an optically thin layer of noble metal. This architecture supports plasmonic "hinge" modes highly localized along the particle's edges and corners, exhibiting Purcell factors exceeding 100 and Q-factors of 15−20 near the plasmon resonance frequency. We demonstrate hinge-mode lasing in submicron $CsPbBr_3$ perovskite cubes encapsulated with conformal 15-nm-thick gold shells. The lasing is achieved with 480-nm nanosecond pumping at 10 pJ/μm^2 through the translucent gold layer, producing a line width of 0.6 at 538 nm. Their rapidly decaying evanescent fields outside the gold coating show distinct sensitivities to long- and short-range external perturbations. Our results suggest the potential of these novel laser modes for sensing and imaging applications.

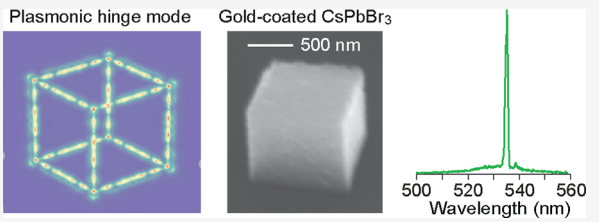

KEYWORDS: *Nanolaser, Plasmonic, Hinge mode, Perovskite, Purcell effect, Imaging*

Plasmonic lasers utilize surface plasmon polaritons (SPPs) at the interface between metals and high-gain media to achieve lasing.[1−16] The Purcell effect enhances the interaction between the plasmonic modes and the gain medium within a small volume to overcome absorption and radiation losses. This process enables lasing from resonators with subwavelength volumes. The most common device structure for plasmonic lasers is the semiconductor-insulator−metal (SIM) configuration, where a semiconductor gain medium is paired with a flat metal substrate separated by an insulating layer. This approach has facilitated plasmonic lasing across a wide range of wavelengths, from ultraviolet to near-infrared, using various semiconductor materials and noble metals.

Recently, there has been growing interest in developing micro- and submicron-sized lasers in particle forms, referred to as laser particles (LPs), for biomedical applications such as cell tracking and single-cell analysis.[17−21] The narrow laser emission, compared to fluorescence, is advantageous for creating extensive color palettes for combinatorial barcoding of individual cells and multiplexing. While particle sizes of 1−2 μm have been found to minimally perturb cells and exhibit low cytotoxicity, smaller sizes are desirable for associating multiple particles with cells[19,20] and for tagging subcellular structures. Among conventional semiconductor materials, metal-halide perovskite offers potential to produce LPs through large-scale, low-cost solution-based methods.[22−24] Our previous work with $CsPbBr_3$ gain media on semi-infinite gold substrates demonstrated submicron perovskite lasers.[3] This result inspired us to explore a new design where $CsPbBr_3$ gain particles are entirely encapsulated by metal.

In this Letter, we present our theoretical and experimental results on gold-coated $CsPbBr_3$ nanolasers, focusing on the characteristics of their lasing modes in the three-dimensional core−shell structure. Our research reveals plasmonic "hinge" modes, which are localized along the 90-deg folded hinges of the metal shell near the plasmon resonance frequency and have an advantage over traditional surface or bulk plasmonic modes, leading to lasing at lower thresholds than other bulk and surface modes. The hinge modes are similar to channel plasmon polaritons (CPP) previously studied in plasmonic waveguides[25,26] and nanowires placed on gold V-grooves.[27] Further, from the perspective of plasmon polaritons tightly bound to the metal-semiconductor interfaces, the semiconductor-core metal-shell architecture is analogous to three-dimensional topological insulators,[28,29] which guide the hinge as well as surface modes. While topological edge-mode lasers have been realized in flat 2D-like structures,[30−33] lasing of hinge modes, either topological or plasmonic, in 3D structures has not been reported.

Figure 1a illustrates the schematic of a semiconductor cube coated with dielectric insulator and metal. When the gold shell's thickness is approximately equal to the skin depth of the metal or less, it is translucent. Therefore, external optical pumping may be used to excite the semiconductor gain medium, allowing the amplification of SPP waves in the gold-semiconductor interface. The dielectric insulator, with a thickness of approximately 5 nm, plays a critical role of reducing carrier quenching from the semiconductor core to the gold shell. This study concentrates on the $CsPbBr_3$ gain

Received: July 20, 2024
Revised: August 24, 2024
Accepted: August 27, 2024
Published: October 16, 2024

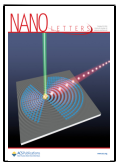

https://doi.org/10.1021/acs.nanolett.4c03485
Nano Lett. 2024, 24, 13647−13652

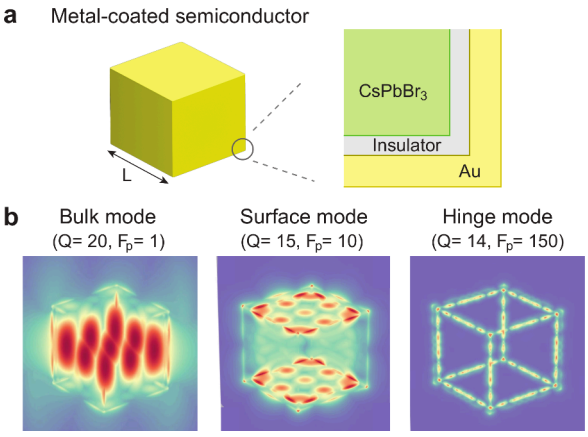

Figure 1. Theoretical cavity modes of a metal-coated perovskite particle. (a) Schematic of a perovskite semiconductor particle encapsulated by an insulator layer, followed by an outer gold shell. (b) Three distinct types of modes (left: Bulk hybrid, middle: Surface, and right: Hinge modes) supported within the metal-coated laser particle with a side length (L) of 400 nm and a gold thickness of 15 nm. These modes are observed in the $CsPbBr_3$'s gain range between 520 and 545 nm.

medium, which exhibits a gain peak around 540 nm.[34] This wavelength is close to the dispersion asymptote of gold SPP for maximizing field localization, considering the perovskite's refractive index (n) of 2.3.

Figure 1b shows three distinct types of modes supported by the structure, identified through Finite Difference Time Domain (FDTD) simulations of a perovskite cube with a side length (L) of 400 nm and a gold thickness of 15 nm. The bulk mode is spread over the volume, while the surface and hinge modes are particularly confined to the sides and edges, respectively. The hinge mode is characterized by opposing charges on the facing gold layers (Figure S1), similar to CPP waves[25,26] in metal bracket waveguides and short-range SPP waves[35] in metal−insulator−metal waveguides.[36−39] The hinge modes form Fabry−Perot-type resonance in the three-dimensional structure. The quality factor (Q) of the hinge mode is comparable to those of the bulk and surface modes. However, the significantly smaller mode volume of the hinge mode offers a greatly higher Purcell factor (F_p). We introduce a figure-of-merit (FOM), defined by the product of these two factors for evaluating the performance of nanoscale lasers: $FOM = Q^*F_p$. According to a simple laser theory (see Note S1),[3] this FOM is inversely related to the spatially averaged carrier density at the lasing threshold (ρ_{th}): $Q^*F_p \approx \omega_0/\rho_{th}V$, where ω_0 represents the mode frequency and V denotes the effective volume of the gain medium. Here it was assumed that the threshold carrier density is much higher than the carrier density to reach the optical transparency in the perovskite ($<10^{18}$ cm^{-3}). The FOM of the hinge mode is calculated to be approximately 2100, significantly higher than 20 for the bulk mode and 150 for the surface mode, highlighting its potential for lasing at lower thresholds.

Using FDTD, we examined how the thickness of the gold layer impacts the properties of the hinge modes across a thickness range from zero (uncoated) to 100 nm. At the interface with the perovskite, the theoretical skin depth is 12 nm, while the skin depth at the air-facing interface is 17 nm. Figure 2 shows simulation results for a $CsPbBr_3$ core with a dimension of 600 nm by 600 nm by 200 nm. Notably, field localization at the hinges is pronounced for gold thicknesses of 15 and 50 nm (Figure 2a). The resonance peak wavelength, starting at 510 nm for optically thick gold, undergoes increasing red-shifts with decreasing gold thickness, moving toward 570 nm at nearly zero gold thickness (Figure 2b).[40] The Q factor experiences a decrease 18 for thick gold to 10 at zero thickness (Figure 2c). The Purcell factor peaks at approximately 200 for gold layers around 10 nm thick but drops sharply for thinner and thicker layers[41] (Figure 2d). When the dielectric insulation layer is introduced between metal and perovskite, the Purcell factor drops to 100 for an insulator thickness of 5 nm and reaches near unity for the insulator thickness of 15 nm. To estimate the efficiency of optical pumping through the metal layer, we calculate the

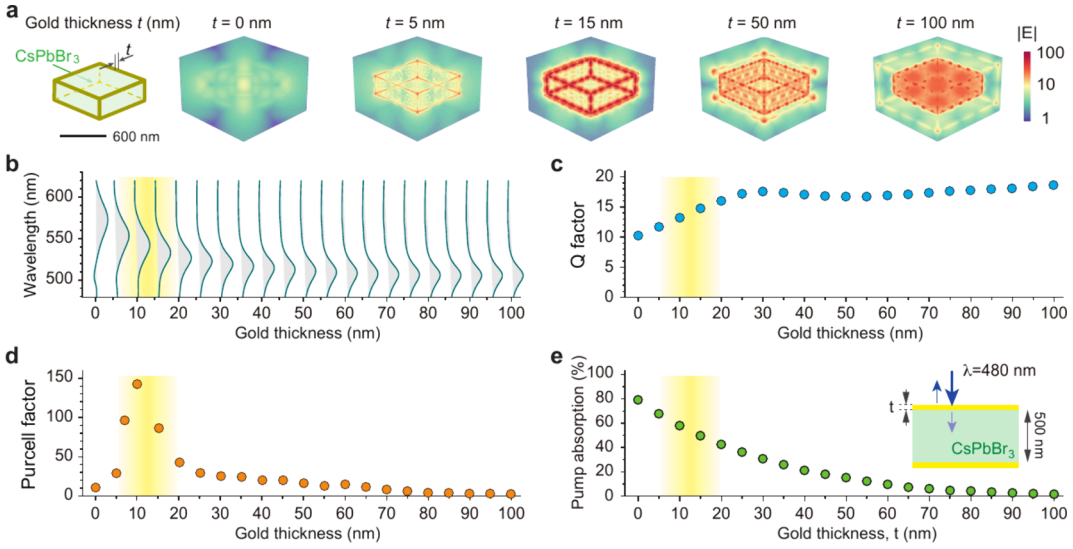

Figure 2. Impact of the gold-shell thickness. (a) The electrical field profiles (|E| in a logarithmic scale) for particles with different gold thicknesses from 0 (no gold) to 100 nm. (b) Mie-scattering profiles; (c) Q factors; (d) Purcell factors for a perovskite size of 600 × 600 × 200 nm depicted in (a). (e) Percentage absorbance of 480-nm pump energy within the perovskite core. Inset, schematic of the model used in (e). The yellow bands shown in (b)−(e) indicate an approximately optimal gold thickness range of 7−18 nm.

https://doi.org/10.1021/acs.nanolett.4c03485
Nano Lett. 2024, 24, 13647−13652

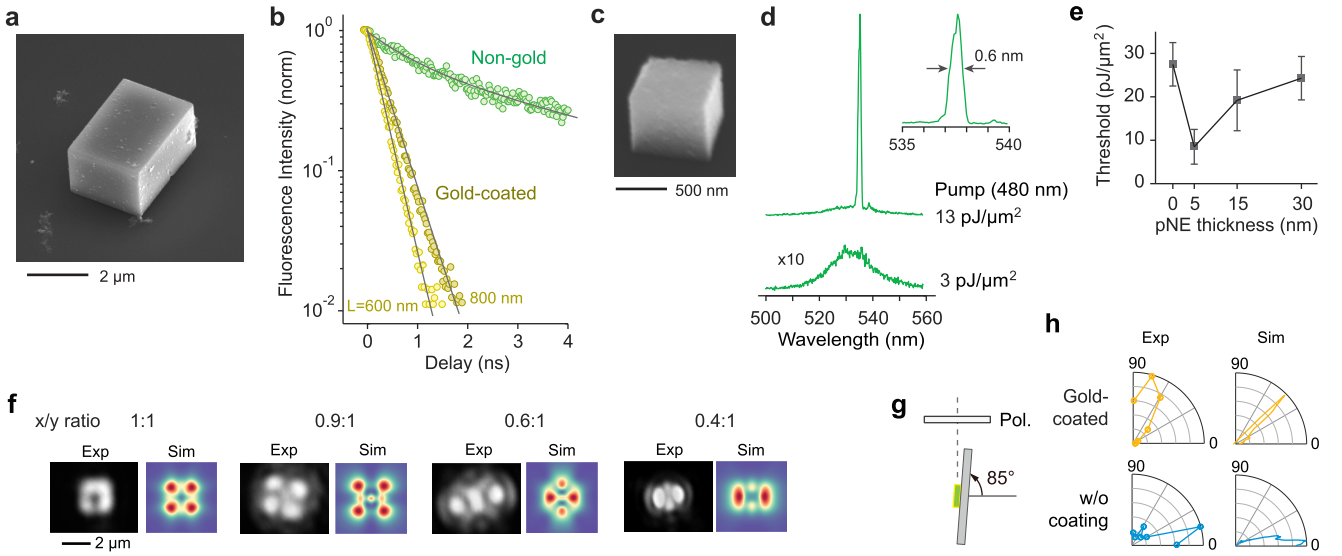

Figure 3. Laser output characteristics. (a) SEM image of a gold-coated $CsPbBr_3$ microparticle. (b) Time-resolved photoluminescence decay of gold-coated particles versus nongold coated particles. Lines show double-exponential fits. (c) Image of a submicron lasing sample. (d) Output emission spectra from the device in (c) pumped by 480-nm nanosecond laser. (e) Measured threshold pump fluence for samples with different pNE layer thicknesses. Error bars indicate the standard deviation of five samples per group. (f) Far-field intensity profiles from four samples with different aspect ratios, compared to FDTD simulation results. (g) Schematic of the polarization measurement setup. (h) Comparison of simulated (sim) and experimentally (exp) measured output polarization states from gold-coated and uncoated samples.

absorbed pump energy in a 500-nm-thick gain slab between two metal layers. For a pumping wavelength of 480 nm, the absorption by the perovskite core starts at 80% without metal, with the rest 20% accounting for both the reflection and transmission of unabsorbed light. The amount of absorption diminishes exponentially with the metal thickness, corresponding to a skin depth of 25 at 480 nm (Figure 2e).

For smaller $CsPbBr_3$ core sizes, the hinge modes are no longer supported. The cutoff of hinge modes occurred at the plasmonic asymptote wavelength of ~510 nm. For example, when one of the side length was reduced from 600 nm, the smallest core sizes that supported hinge modes were approximately 600 × 120 × 200 nm in the simulation (Figures S2 and S3).

Experimentally, $CsPbBr_3$ particles were synthesized using a sonochemistry method, with poly norepinephrine (pNE) layer[42] serving as a dielectric insulating layer before adding a gold-shell coating. This coating was achieved by reducing Au (III) ions with gold nanoparticle seeds (see Note S2). The size of the perovskite crystals was controlled by adjusting the sonochemistry conditions. A scanning electron microscopy (SEM) image shown in Figure 3a reveals a cuboidal-shaped particle, with the pNE and gold layers aimed to be 5 and 15 nm thick, respectively. Compared to nonmetal-coated samples, which exhibited a photoluminescence decay time of ~ 150 ns, the gold-coated samples demonstrated significantly accelerated decays (Figure 3b), with a lifetime of 0.83 ns corresponding to a Purcell factor of 180 (Table S1). The fluorescence quantum yield of uncoated $CsPbBr_3$ microcrystals was previously recorded at 1.5% due to defects created during the sonochemistry process.[42] The Purcell-enhanced emission is thought to increase the quantum yield to nearly 100% during laser oscillation.[3]

The samples were dispersed on thermal-oxide silicon substrates and exposed to 5-ns pump pulses at 480 nm wavelength. Emissions were analyzed using a hyperspectral microscope at room temperature (Figure S4). Postoptical measurements involved marking particle locations on the substrate with high-energy 480-nm pulses, followed by SEM imaging to determine their particle sizes. Figure 3c shows one of the smallest devices measured (680 × 530 × 490 nm^3) that showed lasing. Notably, pristine $CsPbBr_3$ crystals of similar and even much larger sizes[3] without gold coating did not exhibit lasing. The observed single-mode spectra had a line width of 0.6 nm at pump fluences beyond the threshold (Figure 3d), which is about 40 times narrower than the below-threshold fluorescence (25 nm). The pump threshold fluences measured from several submicron particles ranged 9 ± 4 pJ/μm^2. Despite approximately 50% loss of pump light through the gold layer, the absorbed pump energy at threshold was similar to that of uncoated perovskite particles on a flat gold substrate. Figure 3e shows threshold pump fluences for samples with varying pNE thicknesses, identifying 5 nm as the optimal thickness. Without the pNE layer, the pump threshold increased due to carrier tunneling to the gold.

The far-field intensity patterns observed in the experiments were consistently replicated by the FDTD simulation of hinge modes (Figure 3f). The two-photon excited fluorescence imaging of the samples yielded distinct patterns, markedly different from those of nonmetal-coated counterparts (Figure S5). The experimental setup for measuring far-field polarization states is depicted in Figure 3g. The simulation shows a 45-degree tilt polarization state of the lasing hinge mode with respect to the major axis, whereas the emission polarization from uncoated particles are aligned parallel to the substrate plane as expected from transverse-electric whispering gallery modes (Figure 3h).[13] The experimentally measured polarization profiles agree with these simulation results, although some discrepancy is observed for plasmonic particles presumably due to structural deviation from perfectly symmetric hinges (Figure 3h).

The strong localization of the plasmonic hinge modes and their rapid decay outside the metal suggests that these modes should be insensitive to long-range external perturbations.

https://doi.org/10.1021/acs.nanolett.4c03485
Nano Lett. 2024, 24, 13647−13652

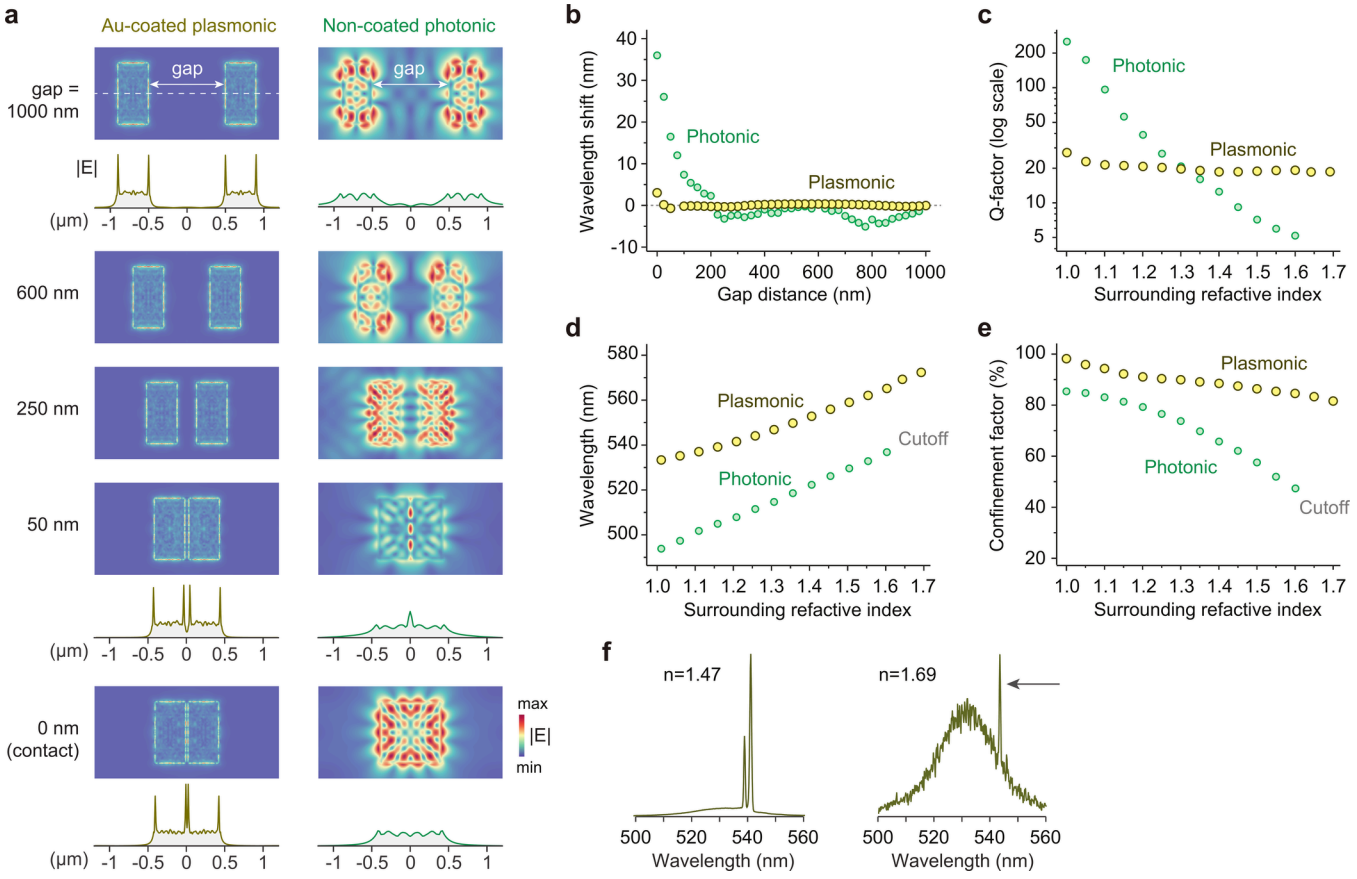

Figure 4. Sensitivity of the plasmonic-hinge and photonic laser modes to external perturbations. (a) Field distributions for the hinge modes of two gold-coated particles (left) and the photonic modes of two uncoated devices (right) in air, across varying intraparticle distances (1000, 600, 250, 50 and 0 nm). (b) Resonance wavelength shifts measured from the simulations in (a). Insets show field amplitude profiles across the mid sections (dashed line in top left picture) for gap distances of 1000, 50, and 0 μm, respectively. (c) Estimated Q-factors; (d) Resonance wavelengths; (e) The fraction of field energy in the gold-perovskite materials for gold-coated (yellow circles) and uncoated (green circles) particles with a side length of 1 μm when immersed in media of different refractive indices. (f) Lasing spectra of two experimental plasmonic LPs when placed in mineral oil (n = 1.47) and poly phenyl ether (PPE) lipid (n = 1.69). Arrow indicates the lasing peak in PPE.

Figure 4a illustrates the resonant mode profiles of two lasing particles as their gap separation progressively decreases to zero. The plasmonic modes showed minimal interactions with nanoscale gaps, and their spatial patterns largely unchanged even at the contact. By contrast, the photonic modes of noncoated particles exhibit dramatic changes as the gap is reduced to less than a half of free-space wavelength. The energy density is localized in the inner surface of the metal, giving significant field energy outside the metal, while the energy is distributed throughout the large particle volume for the photonic mode. Figure 4b illustrates the corresponding evolution of resonant wavelength.

Next, we examined the effect of surrounding index changes on the cavity modes of gold-coated and uncoated particles with a side length of 1 μm. In contrast to photonic modes with Q factors decreasing exponentially with increasing refractive index, the plasmonic hinge mode maintains Q-factor values of 21 to 28 nearly constant across different refractive indices ranging from 1.0 to 1.6 (Figure 4c). Interestingly, as the refractive index was changed, we observed significant wavelength shifts for both hinge and photonic modes (Figure 4d). This is because the surrounding index increases, the fraction of mode energy outside the metal layer increases with the index and changes the cavity boundary conditions (Figure 4e). Experimentally, we achieved lasing of metal-coated LPs immersed in high-index mineral oil (n = 1.47) and poly phenyl ethers (n = 1.69) lipid (Figure 4f).[43] Uncoated photonic LPs, despite being large (up to 4 μm) and stable in organic fluids, did not achieve the lasing threshold in these high refractive-index media.

In conclusion, we have explored plasmonic hinge modes in a semiconductor-core metal-shell structure and investigated their lasing characteristics in gold-coated $CsPbBr_3$ cuboidal particles at room temperature.[39,40] At wavelengths close to the plasmon resonance frequency, the hinge modes are significantly localized at the edges and corners. This localization gives the hinge modes a distinct advantage for lasing in submicron-scale devices. Their narrow-band emission characteristics and range-dependent sensitivity to external perturbations suggest the potential of plasmonic LPs for biological imaging and sensing applications.

■ ASSOCIATED CONTENT

Supporting Information

The Supporting Information is available free of charge at https://pubs.acs.org/doi/10.1021/acs.nanolett.4c03485.

Methods, plasmonic hinge mode in 2D waveguide, laser rate equation model, electric dipole simulation while reducing the particle along its short axis, simulations of Mie scattering by reducing the particle along its long

https://doi.org/10.1021/acs.nanolett.4c03485
Nano Lett. 2024, 24, 13647−13652

axis, gold-coated $CsPbB_{r3}$ particle synthesis, experimental setup, two-photon fluorescence imaging, and measured fluorescence decay parameters (PDF)

AUTHOR INFORMATION

Corresponding Author

Seok Hyun Yun − *Wellman Center for Photomedicine, Massachusetts General Hospital and Harvard Medical School, Cambridge, Massachusetts 02139, United States; Harvard-MIT Health Sciences and Technology, Massachusetts Institute of Technology, Cambridge, Massachusetts 02139, United States;* orcid.org/0000-0002-8176-9916; Email: syun@hms.harvard.edu

Authors

Sangyeon Cho − *Wellman Center for Photomedicine, Massachusetts General Hospital and Harvard Medical School, Cambridge, Massachusetts 02139, United States; Harvard-MIT Health Sciences and Technology, Massachusetts Institute of Technology, Cambridge, Massachusetts 02139, United States;* orcid.org/0000-0002-2997-4760

Yi Yang − *Research Laboratory of Electronics, Massachusetts Institute of Technology, Cambridge, Massachusetts 02139, United States; Department of Physics, University of Hong Kong, Hong Kong 999077, China;* orcid.org/0000-0003-2879-4968

Marin Soljačić − *Research Laboratory of Electronics, Massachusetts Institute of Technology, Cambridge, Massachusetts 02139, United States;* orcid.org/0000-0002-7184-5831

Complete contact information is available at: https://pubs.acs.org/10.1021/acs.nanolett.4c03485

Author Contributions

S.C. and S.H.Y. designed the project. S.C. performed experiments and computer simulation. Y.Y. and M.S. assisted in simulation. S.C. and S.H.Y. wrote the manuscript with input from all authors.

Notes

The authors declare the following competing financial interest(s): S.H.Y. has financial interests in LASE Innovation Inc., a company focused on commercializing technologies based on laser particles. The financial interests of S.H.Y. were reviewed and are managed by Mass General Brigham in accordance with their conflict-of-interest policies.

ACKNOWLEDGMENTS

This study was supported by the US National Institutes of Health research grants (R01EB033155 and R01EB034687). This work was also supported in part by the U.S. Army Research Office through the Institute for Soldier Nanotechnologies at MIT, under Collaborative Agreement Number W911NF-23-2-0121. S.C. acknowledges the MGH fund for medical discovery (FMD) fundamental research fellowship award.

ABBREVIATIONS

SEM, scanning electron microscopy;; FDTD, finite-difference time-domain;; LP, laser particle.

REFERENCES

(1) Berini, P.; De Leon, I. Surface Plasmon-Polariton Amplifiers and Lasers. *Nat Photonics* **2012**, *6* (1), 16−24.

(2) Wang, S.; Wang, X.-Y.; Li, B.; Chen, H.-Z.; Wang, Y.-L.; Dai, L.; Oulton, R. F.; Ma, R.-M. Unusual Scaling Laws for Plasmonic Nanolasers beyond the Diffraction Limit. *Nat Commun* **2017**, *8* (1), 1889.

(3) Cho, S.; Yang, Y.; Soljačić, M.; Yun, S. H. Submicrometer Perovskite Plasmonic Lasers at Room Temperature. *Sci Adv* **2021**, *7* (35), eabf3362.

(4) Cho, S.; Martino, N.; Yun, S.-H. Half-Wave Dipolar Metal-Semiconductor Laser. **2023**, *2310.08742*, *Arxiv*; https://arxiv.org/abs/2310.08742 (accessed 08.19.2024).

(5) Azzam, S. I.; Kildishev, A. V.; Ma, R.-M.; Ning, C.-Z.; Oulton, R.; Shalaev, V. M.; Stockman, M. I.; Xu, J.-L.; Zhang, X. Ten Years of Spasers and Plasmonic Nanolasers. *Light Sci Appl* **2020**, *9* (1), 1−21.

(6) Ma, R.-M.; Oulton, R. F. Applications of Nanolasers. *Nat. Nanotechnol* **2019**, *14*, 12−22.

(7) Khajavikhan, M.; Simic, A.; Katz, M.; Lee, J. H.; Slutsky, B.; Mizrahi, A.; Lomakin, V.; Fainman, Y. Thresholdless Nanoscale Coaxial Lasers. *Nature* **2012**, *482* (7384), 204.

(8) Lu, Y.-J.; Kim, J.; Chen, H.-Y.; Wu, C.; Dabidian, N.; Sanders, C. E.; Wang, C.-Y.; Lu, M.-Y.; Li, B.-H.; Qiu, X.; et al. Plasmonic Nanolaser Using Epitaxially Grown Silver Film. *Science* **2012**, *337* (6093), 450−453.

(9) Kwon, S.-H.; Kang, J.-H.; Seassal, C.; Kim, S.-K.; Regreny, P.; Lee, Y.-H.; Lieber, C. M.; Park, H.-G. Subwavelength Plasmonic Lasing from a Semiconductor Nanodisk with Silver Nanopan Cavity. *Nano Lett* **2010**, *10* (9), 3679−3683.

(10) Hill, M. T.; Oei, Y.-S.; Smalbrugge, B.; Zhu, Y.; de Vries, T.; van Veldhoven, P. J.; van Otten, F. W. M.; Eijkemans, T. J.; Turkiewicz, J. P.; de Waardt, H.; Geluk, E. J.; Kwon, S.-H.; Lee, Y.-H.; Nötzel, R.; Smit, M. K. Lasing in Metallic-Coated Nanocavities. *Nat Photonics* **2007**, *1*, 589−594.

(11) Zhang, Q.; Li, G.; Liu, X.; Qian, F.; Li, Y.; Sum, T. C.; Lieber, C. M.; Xiong, Q. A Room Temperature Low-Threshold Ultraviolet Plasmonic Nanolaser. *Nat Commun* **2014**, *5*, 4953.

(12) Sidiropoulos, T. P. H.; Röder, R.; Geburt, S.; Hess, O.; Maier, S. A.; Ronning, C.; Oulton, R. F. Ultrafast Plasmonic Nanowire Lasers near the Surface Plasmon Frequency. *Nat Phys* **2014**, *10* (11), 870−876.

(13) Ma, R.-M.; Oulton, R. F.; Sorger, V. J.; Bartal, G.; Zhang, X. Room-Temperature Sub-Diffraction-Limited Plasmon Laser by Total Internal Reflection. *Nat. Mater.* **2011**, *10* (2), 110−113.

(14) Oulton, R. F.; Sorger, V. J.; Zentgraf, T.; Ma, R.-M.; Gladden, C.; Dai, L.; Bartal, G.; Zhang, X. Plasmon Lasers at Deep Subwavelength Scale. *Nature* **2009**, *461* (7264), 629−632.

(15) Yang, S.; Bao, W.; Liu, X.; Kim, J.; Zhao, R.; Ma, R.; Wang, Y.; Zhang, X. Subwavelength-Scale Lasing Perovskite with Ultrahigh Purcell Enhancement. *Matter* **2021**, *4* (12), 4042−4050.

(16) Zhou, W.; Dridi, M.; Suh, J. Y.; Kim, C. H.; Co, D. T.; Wasielewski, M. R.; Schatz, G. C.; Odom, T. W. Lasing Action in Strongly Coupled Plasmonic Nanocavity Arrays. *Nat Nanotechnol* **2013**, *8* (7), 506.

(17) Martino, N.; Kwok, S. J. J.; Liapis, A. C.; Forward, S.; Jang, H.; Kim, H.-M.; Wu, S. J.; Wu, J.; Dannenberg, P. H.; Jang, S.-J.; Lee, Y.-H.; Yun, S.-H. Wavelength-Encoded Laser Particles for Massively-Multiplexed Cell Tagging. *Nat Photonics* **2019**, *13* (10), 720−727.

(18) Schubert, M.; Woolfson, L.; Barnard, I. R. M.; Dorward, A. M.; Casement, B.; Morton, A.; Robertson, G. B.; Appleton, P. L.; Miles, G. B.; Tucker, C. S.; et al. Monitoring Contractility in Cardiac Tissue with Cellular Resolution Using Biointegrated Microlasers. *Nat Photonics* **2020**, *14* (7), 452−458.

(19) Fikouras, A. H.; Schubert, M.; Karl, M.; Kumar, J. D.; Powis, S. J.; Di Falco, A.; Gather, M. C. Non-Obstructive Intracellular Nanolasers. *Nat Commun* **2018**, *9* (1), 4817.

(20) Sarkar, D.; Cho, S.; Yan, H.; Martino, N.; Dannenberg, P. H.; Yun, S. H. Ultrasmall InGa(As)P Dielectric and Plasmonic Nanolasers. *ACS Nano* **2023**, *17*, 16048−16055.

(21) Kwok, S. J. J.; Forward, S.; Fahlberg, M. D.; Assita, E. R.; Cosgriff, S.; Lee, S. H.; Abbott, G. R.; Zhu, H.; Minasian, N. H.; Vote, A. S.; Martino, N.; Yun, S.-H. High-Dimensional Multi-Pass Flow Cytometry via Spectrally Encoded Cellular Barcoding. *Nat Biomed Eng* **2024**, *8* (3), 310−324.
(22) Cho, S.; Yun, S. H. Structure and Optical Properties of Perovskite-Embedded Dual-Phase Microcrystals Synthesized by Sonochemistry. *Commun Chem* **2020**, *3* (1), 1−7.
(23) Moon, J.; Mehta, Y.; Gundogdu, K.; So, F.; Gu, Q. Metal-Halide Perovskite Lasers: Cavity Formation and Emission Characteristics. *Advanced Materials* **2024**, *36*, 2211284.
(24) Zhang, Q.; Shang, Q.; Su, R.; Do, T. T. H.; Xiong, Q. Halide Perovskite Semiconductor Lasers: Materials, Cavity Design, and Low Threshold. *Nano Lett* **2021**, *21* (5), 1903−1914.
(25) Bozhevolnyi, S. I.; Volkov, V. S.; Devaux, E.; Ebbesen, T. W. Channel Plasmon-Polariton Guiding by Subwavelength Metal Grooves. *Phys. Rev. Lett.* **2005**, *95* (4), No. 046802.
(26) Moreno, E.; Garcia-Vidal, F. J.; Rodrigo, S. G.; Martin-Moreno, L.; Bozhevolnyi, S. I. Channel Plasmon-Polaritons: Modal Shape, Dispersion, and Losses. *Opt. Lett.* **2006**, *31* (23), 3447−3449.
(27) Bermúdez-Ureña, E.; Tutuncuoglu, G.; Cuerda, J.; Smith, C. L. C.; Bravo-Abad, J.; Bozhevolnyi, S. I.; Fontcuberta i Morral, A.; García-Vidal, F. J.; Quidant, R. Plasmonic Waveguide-Integrated Nanowire Laser. *Nano Lett* **2017**, *17* (2), 747−754.
(28) Schindler, F.; Cook, A. M.; Vergniory, M. G.; Wang, Z.; Parkin, S. S. P.; Bernevig, B. A.; Neupert, T. Higher-Order Topological Insulators. *Sci Adv* **2018**, *4* (6), No. eaat0346.
(29) Fu, L.; Kane, C. L.; Mele, E. J. Topological Insulators in Three Dimensions. *Phys. Rev. Lett.* **2007**, *98* (10), 106803.
(30) Bahari, B.; Ndao, A.; Vallini, F.; El Amili, A.; Fainman, Y.; Kanté, B. Nonreciprocal Lasing in Topological Cavities of Arbitrary Geometries. *Science* **2017**, *358* (6363), 636−640.
(31) Harari, G.; Bandres, M. A.; Lumer, Y.; Rechtsman, M. C.; Chong, Y. D.; Khajavikhan, M.; Christodoulides, D. N.; Segev, M. Topological Insulator Laser: Theory. *Science* **2018**, *359* (6381), No. eaar4003.
(32) Bandres, M. A.; Wittek, S.; Harari, G.; Parto, M.; Ren, J.; Segev, M.; Christodoulides, D. N.; Khajavikhan, M. Topological Insulator Laser: Experiments. *Science* **2018**, *359* (6381), No. eaar4005.
(33) Kim, H.-R.; Hwang, M.-S.; Smirnova, D.; Jeong, K.-Y.; Kivshar, Y.; Park, H.-G. Multipolar Lasing Modes from Topological Corner States. *Nat. Commun.* **2020**, *11* (1), 5758.
(34) Geiregat, P.; Maes, J.; Chen, K.; Drijvers, E.; De Roo, J.; Hodgkiss, J. M.; Hens, Z. Using Bulk-like Nanocrystals to Probeintrinsic Optical Gain Characteristics of Inorganic Lead Halide Perovskites. *ACS Nano* **2018**, *12* (10), 10178−10188.
(35) Woolf, D.; Loncar, M.; Capasso, F. The Forces from Coupled Surface Plasmon Polaritons in Planar Waveguides. *Opt Express* **2009**, *17* (22), 19996−20011.
(36) Dintinger, J.; Martin, O. J. F. Channel and Wedge Plasmon Modes of Metallic V-Grooves with Finite Metal Thickness. *Opt Express* **2009**, *17* (4), 2364−2374.
(37) Celebrano, M.; Wu, X.; Baselli, M.; Großmann, S.; Biagioni, P.; Locatelli, A.; De Angelis, C.; Cerullo, G.; Osellame, R.; Hecht, B.; et al. Mode Matching in Multiresonant Plasmonic Nanoantennas for Enhanced Second Harmonic Generation. *Nat Nanotechnol* **2015**, *10* (5), 412−417.
(38) Bozhevolnyi, S. I.; Volkov, V. S.; Devaux, E.; Laluet, J.-Y.; Ebbesen, T. W. Channel Plasmon Subwavelength Waveguide Components Including Interferometers and Ring Resonators. *Nature* **2006**, *440* (7083), 508−511.
(39) Chen, J.; Smolyakov, G. A.; Brueck, S. R. J.; Malloy, K. J. Surface Plasmon Modes of Finite, Planar, Metal-Insulator-Metal Plasmonic Waveguides. *Opt Express* **2008**, *16* (19), 14902−14909.
(40) Dionne, J. A.; Sweatlock, L. A.; Atwater, H. A.; Polman, A. Plasmon Slot Waveguides: Towards Chip-Scale Propagation with Subwavelength-Scale Localization. *Phys Rev B* **2006**, *73* (3), 35407.
(41) Yang, Y.; Zhen, B.; Hsu, C. W.; Miller, O. D.; Joannopoulos, J. D.; Soljačić, M. Optically Thin Metallic Films for High-Radiative-Efficiency Plasmonics. *Nano Lett* **2016**, *16* (7), 4110−4117.
(42) Cho, S.; Yun, S. H. Poly (Catecholamine) Coated CsPbBr3 Perovskite Microlasers: Lasing in Water and Biofunctionalization. *Adv Funct Mater* **2021**, *31* (27), 2101902.
(43) Nezhad, M. P.; Simic, A.; Bondarenko, O.; Slutsky, B.; Mizrahi, A.; Feng, L.; Lomakin, V.; Fainman, Y. Room-Temperature Subwavelength Metallo-Dielectric Lasers. *Nat Photonics* **2010**, *4*, 395−399.

https://doi.org/10.1021/acs.nanolett.4c03485
Nano Lett. 2024, 24, 13647−13652